nature portfolio

Peer Review File

Regular-wrinkling tunable MXene lattice for electromagnetic interference shielding

Corresponding Author: Professor Guang-Sheng Wang

This file contains all reviewer reports in order by version, followed by all author rebuttals in order by version.

Version 0:

Reviewer comments:

Reviewer #1

(Remarks to the Author)
In this manuscript, the authors proposed a homogeneous strain strategy to achieve self-wrinkling-induced lattice-structured MXene by uniform polymer shrinkage due to dehydration, which is an interesting and novel research result and has certain significance in this field. I believe that with some minor modifications, this manuscript satisfies the standards of Nature Communications.
1. The author blade-coated the concentrated MXene solution onto the PAA surface. Was the PAA in a solid state or gel state during the blade-coating process, and does the PAA still contain solvent?
2. The article mentions that MXene does not form lattice-like structures on PET, PTFE, PVDF, or glass due to the lack of interaction forces between MXene and these substrates. Does MXene form patterned structures on other polymeric surfaces that can establish bonding interactions with MXene?
3. Figure 1C shows the cross-sectional view of MXene/PI. Is MXene prone to delamination from the PI surface? There is a modulus mismatch between MXene and the polymer. Why do more pronounced wrinkles and protrusions form between MXene and the polymer during shrinkage? Do hydrogen bonds exist between MXene and the polymer after heat treatment?
4. When testing the EMI shielding performance of the lattice-structured MXene, is the PI substrate included? Does the presence of the PI substrate affect the EMI shielding efficiency of the film?
5. Compared to flat structures, lattice structures exhibit higher EMI shielding efficiency. The article mentions that this improvement is due to the increase in additional conductive pathways and surface scattering effects. Which of these two factors has a more significant impact on the EMI shielding performance?
6. Is the MXene/PI film prone to oxidation or delamination when exposed to air, potentially affecting its practical application in real-world environments?
7. Figure 3B elucidates the EMI shielding performance of the MXene/PI film after stretching. Does the MXene/PI film exhibit elastic recovery (return to its original state) after stretching, and can the cracks be healed or repaired?
8. The lattice MXene exhibits a hydrophobic contact angle of 125° due to its surface lattice structure, but it does not reach superhydrophobicity (150°). Has the author attempted further surface energy reduction treatments (e.g., chemical modification or nanostructuring) to achieve superhydrophobicity?

Reviewer #2

(Remarks to the Author)
Manuscript Number: NCOMMS-25-19801-T
Recommendation: Major Revision
The manuscript titled “Regular-wrinkling tunable MXene lattice for electromagnetic interference shielding” presents an interesting approach where PAA film/MXene composites are thermally treated on PI films to fabricate wrinkle-tunable MXene composite film. The structural transformation improved mechanical strength, EMI shielding and Joule heating performance. While the concept is very interesting, the current version of the manuscript lacks clarity in several key areas, making it difficult to fully assess the validity and significance of the findings. Therefore, I would like to recommend a major revision before reconsideration for publication in Nature Communications.
My specific comments are as follows:

1. Precise sample characterization is essential in this study, particularly in maintaining consistent dimensions and electrical

conductivity. However, detailed information is missing. Authors should provide comprehensive data for all samples, including effective thickness (thickness of flat area and thinness of peak area), and corresponding electrical conductivity values.
2. The authors state, "During the high-temperature treatment process, the dehydration cyclization of the PAA leads to uniform contraction of the PI (Fig. S6)." However, Figure S6 depicts only the synthesis process of poly(amic acid) precursors (PAA) and polyimide (PI). The authors should provide supporting evidence for the claim regarding uniform contraction of PI.
3. The authors should report the d-spacing values following the removal of interlayer water from the composite for a more complete analysis.
4. The amplitude presented in Figure S8 does not align with the 2-micron claim. The authors are advised to review this inconsistency.
5. The authors should further clarify this expression: “For an effective comparison of EMI shielding coefficients, the thickness of the flat MXene film should also be provided. Compared with the flat MXene, the reflection loss (SEA) and absorption loss 118 (SER) of the latticed MXene increase by 10.1 dB and 1.7 dB (Table S4), while the absorption coefficient (A) increase by 1% (Fig. S15).”
6. The authors should further clarify how a 1% increase in the absorption coefficient leads to a 31% improvement in EMI shielding performance of the MXene lattice. Moreover, the authors have demonstrated that the lattice structure contributes additional conductive pathways and an increased reflective surface compared to flat MXene, which should be discussed in more detail.
7. The authors should provide experimental electrical conductivity data for latticed, vacuum-filtered, and flat MXene films. In addition, conductivity and EMI SE values calculated using equation 4 and 5 should be included for better comparison and understanding.
8. Author should provide the detail discussion on the multiple reflection effect in this study.
9. The original and retained values of EMI shielding effectiveness (SE) should be included in the text to demonstrate the long-term stability of the latticed MXene structure for better understanding.
10. The term "MXene/PI films" should be clarified: does it refer to latticed MXene or the entire MXene composite? Similarly, the title of Figure 4 should reflect this clarification.
11. In the synthesis section, the authors mention using the HCl/LiF method for fabricating MXene. However, it is unclear why sonication is necessary, as this process is commonly used for synthesizing single-layer MXene.
12. References 19 and 33 appear to be identical and should be revised accordingly.
13. The authors are encouraged to provide detailed discussions for all figures and subfigures in the supporting information section to enhance the overall clarity and completeness of the manuscript.

Version 1:

Reviewer comments:

Reviewer #1

(Remarks to the Author)
Accept.

Reviewer #2

(Remarks to the Author)
Nature Communication
Manuscript Number: nature communctaion-5943640
Recommendation: Major Revision
Although the authors have revised the manuscript as suggested, several critical issues remain. There are still unclear points regarding the main advantages of the lattice-structured MXene in terms of properties compared to the reported literature. In addition, the EMI shielding and Joule heating performance comparisons are still very limited. The authors need to address the following comments:

1. The novelty of this work remains unclear. The enhanced EMI shielding performance largely results from the improved electrical conductivity of the lattice-structured MXene. However, achieving high EMI shielding effectiveness (SE) through increased conductivity is already well established in the literature. No fundamentally new mechanism has been introduced. Similar strategies that combine surface patterning with conductivity enhancement have already been reported, e.g., Angew. Chem. Int. Ed. 2022, 61, e202201323. The authors should clarify the novelty of their approach and how it differs from existing methods.
2. The authors compare the EMI performance with limited literature. However, a more comprehensive benchmarking against state-of-the-art MXene shielding materials, particularly those with thicknesses below 20 μm, is missing. The authors should include a plot of EMI SE versus thickness for pristine MXene reported in the literature in Figure 1f, along with the corresponding numerical data in a supplementary table. This will enable readers to better understand how the lattice-structured MXenes (MXene/PI) in this study compare to previously reported pristine MXene films and allow for a more robust evaluation of their EMI performance.
3. Authors should provide AFM images and thickness profiles of the pristine PAA film (Supplementary Figure 7a) and PI film (Supplementary Figure 7c). This is necessary to assess whether any wrinkles form on the PI film after drying. If the pristine PI film does not exhibit wrinkles, it raises concerns about the interfacial interactions between MXene and PI. In such a scenario, the adhesion at the MXene/PI interface may be significantly weakened upon drying, potentially leading to

delamination or peeling.
4. For Figure S34, the authors should provide a video showing the immersion of the lattice MXene in liquid nitrogen, followed by its bendability after removal. MXene films typically become brittle under such conditions and are prone to breaking upon bending. Including this video would help validate the mechanical flexibility and structural integrity of the lattice MXene under extreme conditions.
5. In Figure 4a, the temperature was measured using an IR camera. However, due to the low IR emissivity of MXene, this method may not provide accurate surface temperature values. The authors should determine the actual IR emissivity of their samples and/or use a contact-mode thermocouple for verification. Additionally, images of the samples after Joule heating at 4 V, 5 V, 6 V, and 7 V should be included to evaluate any morphological or structural changes induced by heating.
6. In Figure 4d, it is unclear why the lattice MXene exhibits higher hydrophobicity and longer icing time. How does the wrinkled structure enhance hydrophobicity? Additionally, what is the significance of the ice sliding off the film at a 20° tilt under 3 V Joule heating? Furthermore, the authors should also compare the Joule heating performance of the vacuum-filtered and flat MXene films at the same voltage. Are the temperature values comparable?

Version 2:

Reviewer comments:

Reviewer #2

(Remarks to the Author)
The authors have addressed the reviewers' comments thoroughly and effectively. Therefore, I recommend the acceptance of this paper.

Response to Reviewers' Comments

Thank you very much for considering our work in the manuscript entitled " Regular-wrinkling tunable MXene lattice for electromagnetic interference shielding "(Full Paper, Manuscript ID NCOMMS-25-19801-T) authored by Shan Zhang, Juntao Wu, Zhi-Ling Hou, Pengfei Hu, Bo Cai, Chenming Liang, Lu Zhou, Wenhao Liang, Yufeng Xue, Martin C. Koo, Pei-Yan Zhao, Li-Min Liu, Mingjie Liu and Guang-Sheng Wang. In addition, we truly appreciate the editor and reviewers for their careful reading of our manuscript and valuable suggestions. The insightful comments have provided us a chance to further improve the quality of our manuscript. The manuscript has been revised in detail according to the comments provided by the reviewers. The changes to the text are highlighted in YELLOW.

The following is our response to the comments of the reviewers

Reviewer 1：

Comments: In this manuscript, the authors proposed a homogeneous strain strategy to achieve self-wrinkling-induced lattice-structured MXene by uniform polymer shrinkage due to dehydration, which is an interesting and novel research result and has certain significance in this field. I believe that with some minor modifications, this manuscript satisfies the standards of Nature Communications.

Reply: Thank you for your positive and constructive comments, which are of great significance for improving the quality and rigor of our manuscript.

Q1: The author blade-coated the concentrated MXene solution onto the PAA surface. Was the PAA in a solid state or gel state during the blade-coating process, and does the PAA still contain solvent?

Reply: The PAA was first dried in an oven at 60°C for 40 minutes to remove the majority of the solvent. At this stage, the PAA exists in a solid state but still retained 25-30% residual solvent. This persistence is attributed to the formation of stable complexes between PAA and DMF[1].

Q2: The article mentions that MXene does not form lattice-like structures on PET, PTFE, PVDF, or glass due to the lack of interaction forces between MXene and these substrates. Does MXene form patterned structures on other polymeric surfaces that can establish bonding interactions with MXene?

Reply: Thanks you for the insightful question. When deposited on a polymer substrate, MXene exhibits a tendency for relative slippage against the substrate under externally applied stress. If bonding interactions exist between MXene and the substrate, the accumulated stress cannot be released through slippage. Instead, it is relieved through buckling deformation. Consequently, MXene forms surface patterns via buckling on polymer surfaces capable of establishing such bonding interactions. This phenomenon extends beyond polyimide substrates.

Q3: Figure 1C shows the cross-sectional view of MXene/PI. Is MXene prone to delamination from the PI surface? There is a modulus mismatch between MXene and the polymer. Why do more pronounced wrinkles and protrusions form between MXene and the polymer during shrinkage? Do hydrogen bonds exist between MXene and the polymer after heat treatment?

Reply: MXene exhibits strong resistance to peeling from the PI surface, as empirically confirmed by the peeling stability test results in Section 3 (Supplementary Fig. 30 and 31) of this work. During the thermal treatment process, PAA undergoes dehydration-induced cyclization to form PI, with stress released through volumetric shrinkage. However, the accumulated stress in MXene cannot be relieved due to its robust bonding with the polymer matrix, consequently manifesting as buckling deformation. Hydrogen bonding between the polymer and MXene is established prior to thermal treatment. During heating, partial dissociation occurs between the original hydrogen bonds connecting PAA and MXene. Following the conversion of PAA to PI via dehydration cyclization, new van der Waals interactions and hydrogen bonds form between the -OH groups on MXene nanosheets and C=O moieties in PI molecular chains.

Q4: When testing the EMI shielding performance of the lattice-structured MXene, is

the PI substrate included? Does the presence of the PI substrate affect the EMI shielding efficiency of the film?

Reply: Thank you for the thought-provoking questions. The electromagnetic interference (EMI) shielding performance of latticed MXene reported in this work includes contributions from the PI substrate. We first measured bare PI and PET films without MXene loading, and their EMI shielding performance is as follows:

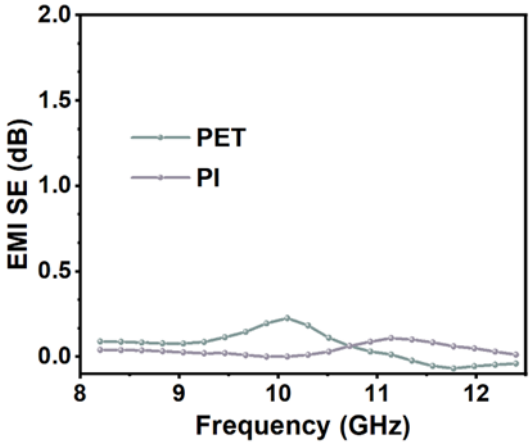

Fig. R1 EMI SE of the PET and PI film.

Results demonstrate that both PI and PET films function as electromagnetically transparent materials, exhibiting negligible EMI shielding performance. This observation aligns with other reported works. Thus, it can be concluded that the presence of PI substrates does not compromise the EMI shielding effectiveness of the composite films.

Q5: Compared to flat structures, lattice structures exhibit higher EMI shielding efficiency. The article mentions that this improvement is due to the increase in additional conductive pathways and surface scattering effects. Which of these two factors has a more significant impact on the EMI shielding performance?

Reply: Thanks you for this intriguing query. According to the test results in Figure 2A, the latticed MXene exhibits enhanced shielding effectiveness by absorption (SE_A) and shielding effectiveness by reflection (SE_R) compared to flat MXene. This indicates that both additional conductive pathways and surface scattering effects contribute to the

EMI shielding performance of the latticed MXene. According to Figure S17, the 1% increase in the reflection coefficient (R) indicates that the additional conductive paths introduced by the lattice structure enhance electrical conductivity. This constitutes the primary contributor to the 31% improvement in EMI SE.

Q6: Is the MXene/PI film prone to oxidation or delamination when exposed to air, potentially affecting its practical application in real-world environments?

Reply: Indeed, oxidation/delamination is a valid concern towards the practicality of the MXene/PI film. Therefore, we conducted experimental tests on the durability of latticed MXene, as in detailed the third and fourth sections of the article. Due to its unique surface structure, MXene with a lattice structure has a hydrophobic angle of 125°, which can effectively prevent contact with water compared to EMI shielding materials without hydrophobic properties, thereby slowing down the oxidation rate. The special lattice structure further enhances the interaction force between MXene and PI, and it does not fall off even after 6 hours of ultrasonic treatment. In conclusion, it is proven that the MXene/PI film is not prone to oxidation or delamination, has good usability, and even has great application prospects in extreme environments.

Q7: Figure 3B elucidates the EMI shielding performance of the MXene/PI film after stretching. Does the MXene/PI film exhibit elastic recovery (return to its original state) after stretching, and can the cracks be healed or repaired?

Reply: Thank you for the interesting question. Since neither PI nor MXene is an elastomer, MXene and PI will retract after stretching and releasing the tension, but they will not return to their original state. The lattice structure can enable MXene/PI films to exhibit stress buffering under small stress/strain, but once cracks occur under large stress, they cannot be repaired. Therefore, the MXene/PI films prepared in this work are suitable for applications in scenarios subject to small stress impacts. In the following work, MXene can be loaded onto an elastomer and self-healing small molecules can be introduced to prepare EMI shielding materials suitable for scenarios subject to large stress impacts.

Q8: The lattice MXene exhibits a hydrophobic contact angle of 125° due to its surface lattice structure, but it does not reach superhydrophobicity (150°). Has the author attempted further surface energy reduction treatments (e.g., chemical modification or nanostructuring) to achieve superhydrophobicity?

Reply: We attempted to deposit perfluorosilane on the surface of the latticed MXene using the vapor deposition method, resulting in a film with a hydrophobic angle of 139°. However, the EMI shielding performance of the film was somewhat reduced (Figure R2). Therefore, in the subsequent work, we considered introducing nano-scale protrusions on the lattice structure to further increase the hydrophobic angle of the film and simultaneously enhance the EMI shielding performance of the material.

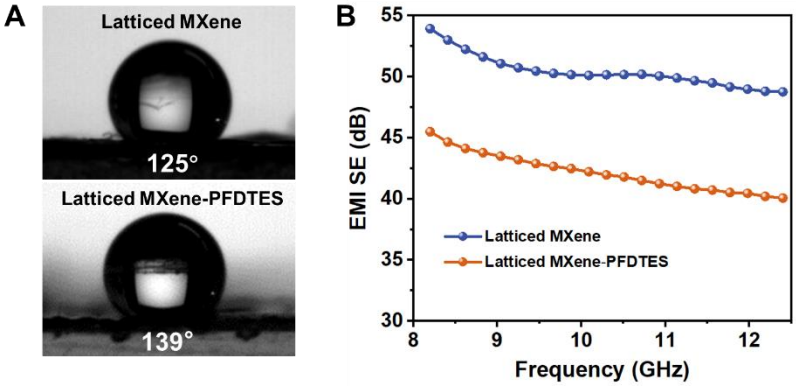

Fig. R2 (A) Water contact angle (B) EMI SE of latticed MXene and latticed MXene-PFDTES.

[1] Brekner, M.-J. et al. *J. Polym. Sci., Part A: Polym. Chem.* **25**: 2005-2020 (1987).

Reviewer 2:

Comments: The manuscript titled "Regular-wrinkling tunable MXene lattice for electromagnetic interference shielding" presents an interesting approach where PAA film/MXene composites are thermally treated on PI films to fabricate wrinkle-tunable MXene composite film. The structural transformation improved mechanical strength, EMI shielding and Joule heating performance. While the concept is very interesting, the current version of the manuscript lacks clarity in several key areas, making it difficult to fully assess the validity and significance of the findings. Therefore, I would like to recommend a major revision before reconsideration for publication in Nature Communications.

Reply: We are very grateful for the recommendation and positive comments made by the reviewer. The concerns of the reviewer are thoroughly addressed in a point-by-point manner as follows, upon which the manuscript is revised accordingly.

Q1: Precise sample characterization is essential in this study, particularly in maintaining consistent dimensions and electrical conductivity. However, detailed information is missing. Authors should provide comprehensive data for all samples, including effective thickness (thickness of flat area and thinness of peak area), and corresponding electrical conductivity values.

Reply: Thank you for your constructive suggestion. The thickness of the samples (thickness of the flat area and the peak area) was measured by scanning electron microscopy (SEM). The cross-sectional SEM images and specific data are presented below. The lattice structure is spontaneously formed, and the flat area and the peak area are the same MXene. It can also be seen from the SEM images that the interlayer spacing of MXene in the flat area and the peak area are practically identical. Combined with the four-probe conductivity meter test, the conductivity values of different points of the lattice MXene film are highly similar, thus it is concluded that the conductivity values of the flat area and the peak area are the same. The conductivity values of different samples are also shown in the table below.

The cross-sectional SEM images of the flat MXene and the latticed MXene mentioned in Figure 2A of the manuscript are as follows:

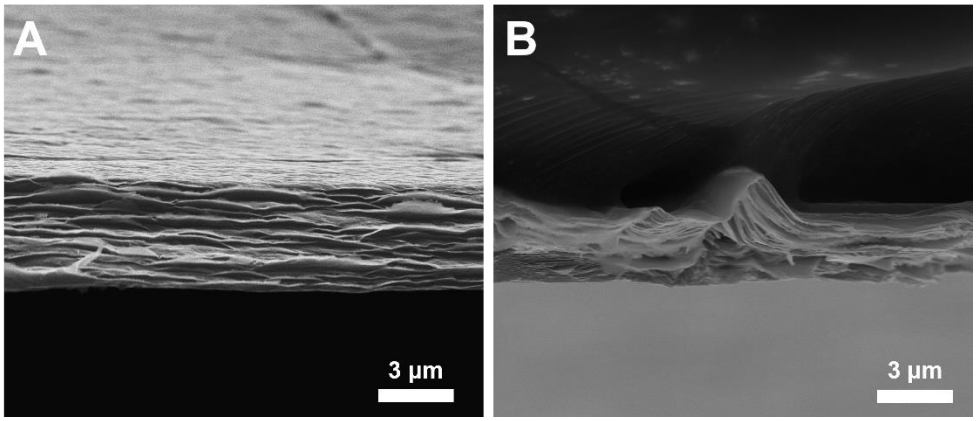

Fig. R3 (Fig. 16 in supplementary information) cross-sectional SEM images of(A) flat MXene, (B) latticed MXene on PI surface.

Table R1 (Supplementary Table 4 in the revised supplementary information) The thickness and electrical conductivity of flat MXene and latticed MXene.

Sample	Thickness of flat area (μm)	Thinness of peak area (μm)	Electrical conductivity (S/cm)
Flat MXene	4.0	0	2500
Latticed MXene	2.8	1.8	3500

In response to this comment, Figure R3 and Table R1 have been added to Figure S16 and Table S4 in the supporting information.

The cross-sectional SEM images of MXene-VAF, flat MXene and latticed MXene mentioned in Figure 2D of the manuscript are as follows:

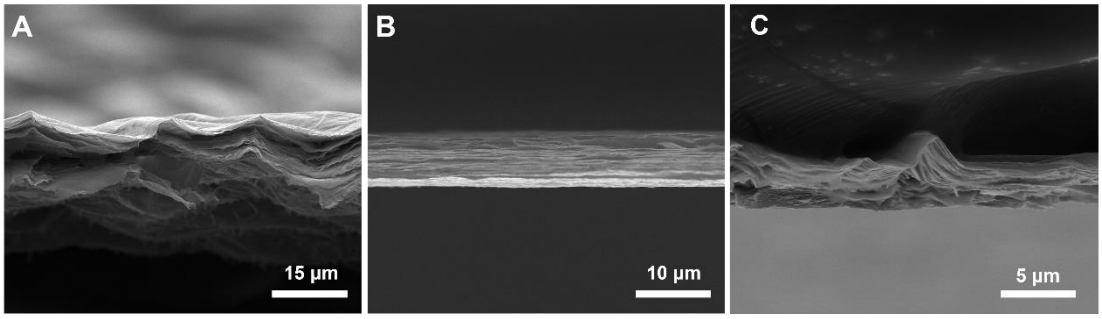

Fig. R4 (Fig. 18 in supplementary information) SEM images of the cross-section for different (A) MXene-VAF, (B) flat MXene and (C) latticed MXene films.

Table R2 (Supplementary Table 6 in the revised supplementary information) The thickness and electrical conductivity of MXene-VAF, flat MXene and latticed MXene.

Sample	Thickness of flat area (μm)	Thinness of peak area (μm)	Electrical conductivity (S/cm)
MXene-VAF	13.0	0	2900
flat MXene	8.0	0	3500
Latticed MXene	2.8	1.8	3500

In response to this comment, Figure R4 and Table R2 have been added to Figure S18 and Table S6 in the supporting information.

The cross-sectional SEM images of latticed MXene films of different thicknesses mentioned in Figure 2E of the manuscript are as follows:

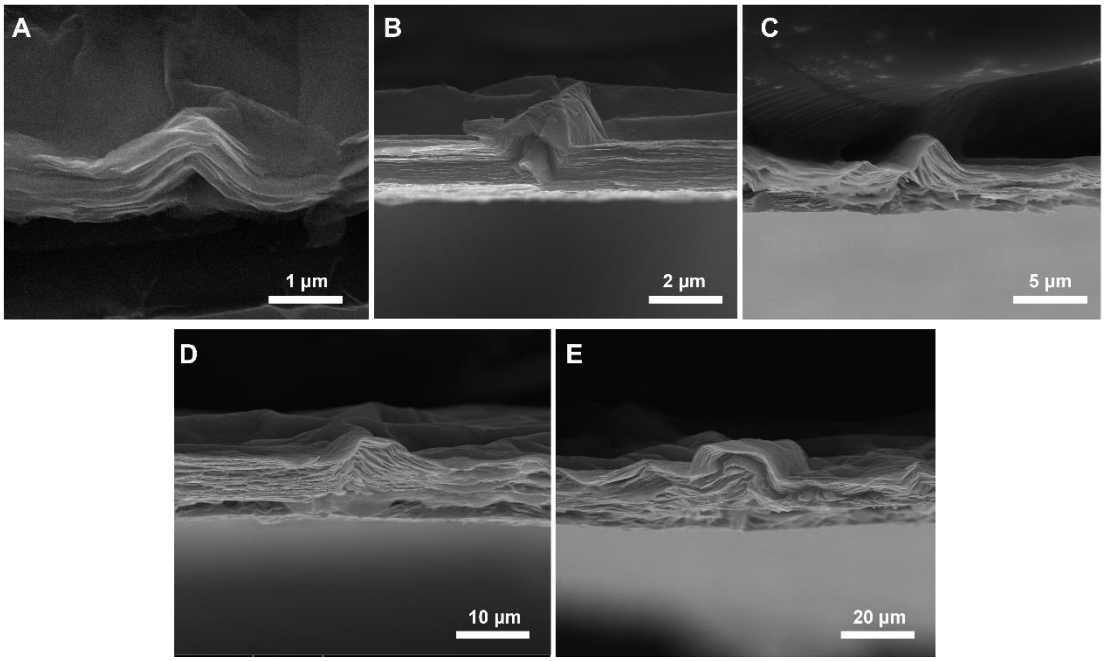

Fig. R5 (Fig. 19 in supplementary information) SEM images of the cross-section for different thicknesses of latticed MXene on PI surface.

Table R3 (Supplementary Table 7 in the revised supplementary information) The thickness and electrical conductivity of the latticed MXene with various thicknesses.

Sample	Thickness of flat area (μm)	Thinness of peak area (μm)	Electrical conductivity (S/cm)
1	0.7	0.5	600
2	1.5	1.0	1000
3	2.8	1.8	3500
4	7.0	3.0	5900
5	17.0	10.0	8000

In response to this comment, Figure R5 and Table R3 have been added to Figure S19 and Table S7 in the supporting information.

Q2: The authors state, "During the high-temperature treatment process, the dehydration cyclization of the PAA leads to uniform contraction of the PI (Fig. S6)." However, Figure S6 depicts only the synthesis process of poly(amic acid) precursors (PAA) and

polyimide (PI). The authors should provide supporting evidence for the claim regarding uniform contraction of PI.

Reply: Thanks you for pointing out this deficiency in the manuscript. We removed PAA/MXene film from the glass substrate and then subjected it to heat treatment. The macroscopic images and cross-sectional SEM images of the PAA before thermal treatment and the PI after thermal imidization are shown below. It can be seen from the figures that the area of PAA before thermal treatment was 6×6 cm and the thickness was 35 μm; after thermal treatment, the area was 5.4×5.4 cm and the thickness was 30 μm. This proves that the process of PAA ring formation and dehydration results in uniform volume contraction.

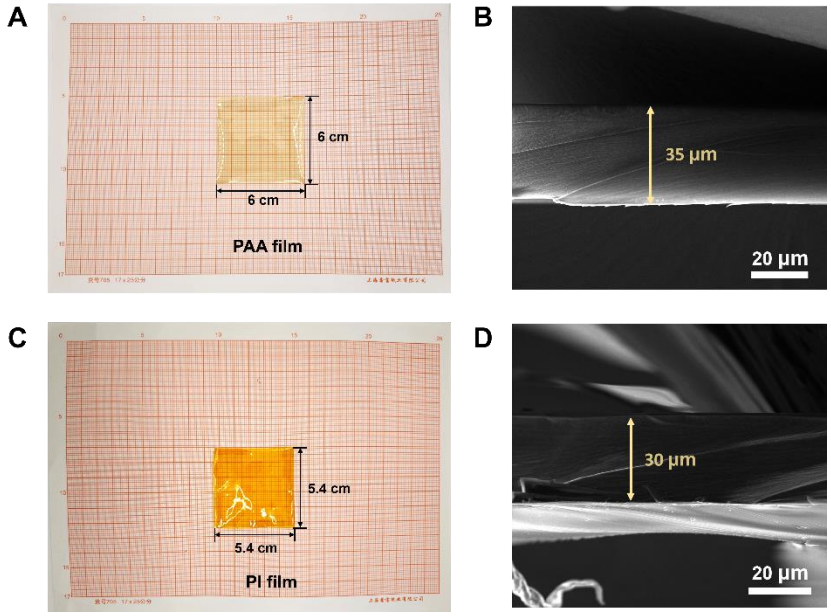

Fig. R6 (Fig. 7 in supplementary information) (A) PAA film on grid paper (6×6 cm). (B) SEM images of the cross-section for PAA film. (C) PI film on grid paper (5.4×5.4 cm). (D) SEM images of the cross-section for PI film.

In response to this comment, Figure R6 have been added to Figure S7 in the supporting information.

Q3: The authors should report the d-spacing values following the removal of interlayer water from the composite for a more complete analysis.

Reply: Thanks you for the excellent suggestion. The heat treatment process at 300°C can effectively remove the interlayer water molecules of MXene. According to Figure R7A, the (002) peak position of MXene on the PAA surface is $2\theta_{peak}$=7.2°. Using Bragg law and Cu Kα radiation (λ=1.5418A), the d-spacing is calculated as follows:

$$\theta = \frac{2\theta_{peak}}{2} = \frac{7.2^\circ}{2} = 3.6^\circ$$

$$\sin(3.6^\circ) \approx 0.0628$$

$$d = \frac{\lambda}{2\sin\theta} = \frac{1.5418}{2\times 0.0628} = \frac{1.5418}{0.1256} \approx 1.23 \text{ nm}$$

The d-spacing of MXene on the PAA surface is approximately 1.23 nm.

The (002) peak position of MXene on the PI surface is $2\theta_{peak}$=8.2°. According to Bragg law and Cu Kα radiation (λ=1.5418 A), the d-spacing is calculated as follows:

$$\theta = \frac{2\theta_{peak}}{2} = \frac{8.2^\circ}{2} = 4.1^\circ$$

$$\sin(4.1^\circ) \approx 0.0715$$

$$d = \frac{\lambda}{2\sin\theta} = \frac{1.5418}{2\times 0.0715} = \frac{1.5418}{0.1430} \approx 1.08 \text{ nm}$$

The d-spacing of MXene on the PI surface is approximately 1.08 nm.

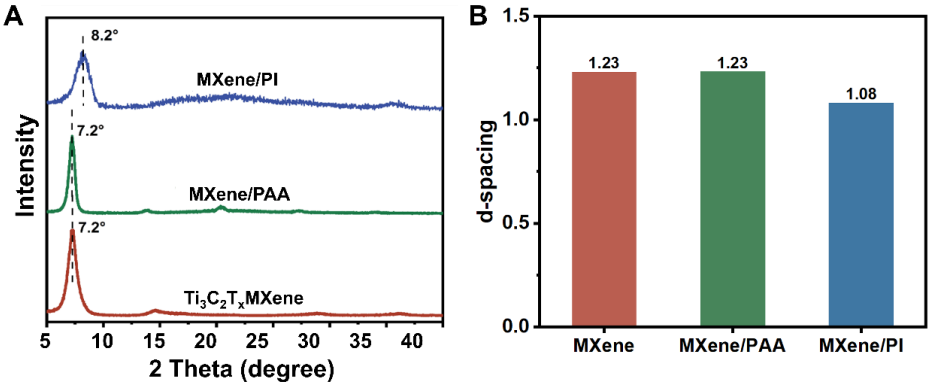

Fig. R7 (Fig. 8 in supplementary information) (A) The XRD patterns and (B) comparison of d-spacing values of MXene, MXene/PAA and MXene/PI films.

In response to this comment, Figure R7 have been added to Figure S8 in the supporting

information. The revised version includes the changes in the MXene layer spacing before and after heat treatment.

Page 5, Paragraph 1, Line 5 in the revised manuscript:

As a result, the MXene coating shrinks further inward on the PI surface, with the MXene layer spacing decreasing from 1.23 to 1.08 nm (Fig. S8), and the amplitude of the lattices increases to 1~2 μm (Fig. S9)

Q4: The amplitude presented in Figure S8 does not align with the 2-micron claim. The authors are advised to review this inconsistency.

Reply: Thank you for pointing out the lack of clarity regarding the 2-micron claim. The AFM images of MXene on PI are presented in Figure R8A (in the manuscript, 1E), and the height statistics are shown in Figure R8B. From the Figure R8B, the amplitude of MXene on PI is 1-2 μm. The cross-sectional SEM image in the supplementary information S9 was tilted, which may have errors. The cross-sectional SEM of MXene on PI are re-tested and the results are shown in Figures R8C and D. The statement in the article that the amplitude of MXene on PI is 2 μm is also not very rigorous. Therefore, we changed the corresponding position in the main text to an amplitude of 1-2 μm.

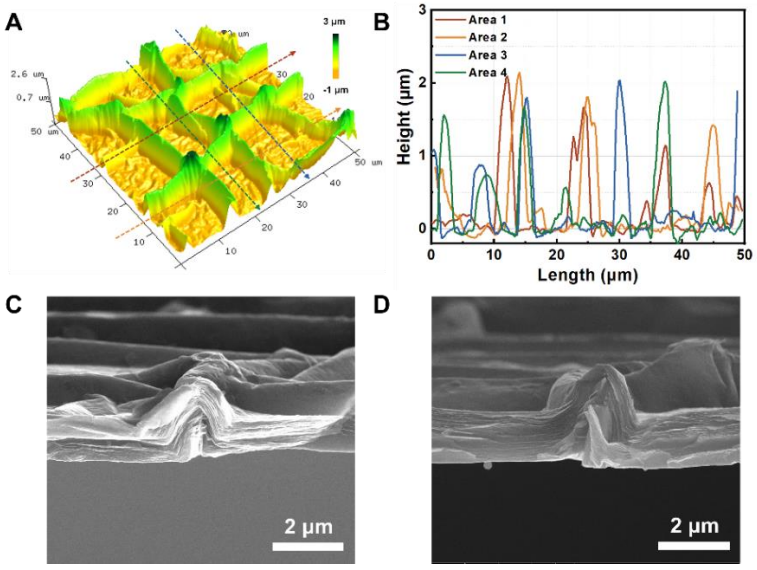

Fig. R8 (Fig. 9 in Supplementary information) (**A**) AFM 3D images with (**B**) height profiles of the latticed MXene on PI surface. (**C, D**) SEM images of the cross-section

for latticed MXene on PI surface.

In response to this comment, Figures R8B, C and D have been added to Figure S9 in the supporting information. The revised version includes the variation in the amplitude height of latticed MXene.

Page 5, Paragraph 2, Line 7 in the revised manuscript:

As a result, the MXene coating shrinks further inward on the PI surface, with the MXene layer spacing decreasing from 1.23 to 1.08 nm (Fig. S8), and the amplitude of the lattices increases to 1-2 μm (Fig. S9)

Q5: The authors should further clarify this expression: "For an effective comparison of EMI shielding coefficients, the thickness of the flat MXene film should also be provided. Compared with the flat MXene, the reflection loss (SEA) and absorption loss (SER) of the latticed MXene increase by 10.1 dB and 1.7 dB (Table S4), while the absorption coefficient (A) increase by 1% (Fig. S15)."

Reply: Thanks you for the constructive suggestion. The thickness of the flat MXene film is shown in Figure R3 (Fig. S16) and Table R1 (Table S4). Re-examination of the reflectance (R) and absorptance (A) values for flat and lattice MXene films identified an error in previous computations. The corrected results show that the 98% R and 2% A for lattice MXene. Compared with the flat MXene (with R is 97% and A is 3%), the R value of lattice MXene increased by 1%. Updated bar plots comparing the R and A of flat and lattice MXene are now provided in Supplementary Figure S17. Compared with the flat MXene, the reflection loss (SE_A) and absorption loss (SE_R) of the latticed MXene increase by 10.3 dB and 1.7 dB (Table S5). This demonstrates that the enhanced EMI SE of the latticed MXene stems from both the improved SE_R due to enhanced electrical conductivity and the increased SE_A resulting from the surface structure promoting diffuse reflection of electromagnetic waves. The core conclusion-that enhanced EMI shielding in lattice MXene stems from concurrent improvements in both reflection and absorption-remains valid. Critically, the 1% increase in reflectance (R) indicates that the primary cause of enhanced electromagnetic interference lies in the

improved electrical conductivity resulting from additional conductive paths introduced by the lattice structure, which subsequently enhances the reflection of electromagnetic waves.

In response to this comment, the revised version includes a comparison and analysis of the conductance data of flat and latticed MXene, as well as the reasons and dominant factors for the increase in the EMI SE value of latticed MXene.

Page 5, Paragraph 4, Line 32-35, in the revised manuscript:

Electrical conductivity is a critical parameter for evaluating the EMI shielding performance of MXene. Firstly, the conductivity of flat MXene on PET and lattice MXene on PI under the same preparation conditions is measured. The latticed MXene exhibited a higher conductivity of 3500 S/cm compared to 2500 S/cm for the flat MXene (Fig. S16 and Table S4).

Page 6, Paragraph 1, Line 4-7, in the revised manuscript:

This demonstrates that the enhanced EMI SE of the latticed MXene stems from both the improved SE_R due to enhanced electrical conductivity and the increased SE_A resulting from the surface structures responsible for promoting diffuse reflection of electromagnetic waves.

Meanwhile, we have included the conductivity data (Fig. S16 and Table S4) and updated bar plots of A and R coefficients and data (Fig. S17 and Table S5) in the supplementary information.

Q6: The authors should further clarify how a 1% increase in the absorption coefficient leads to a 31% improvement in EMI shielding performance of the MXene lattice. Moreover, the authors have demonstrated that the lattice structure contributes additional conductive pathways and an increased reflective surface compared to flat MXene, which should be discussed in more detail.

Reply: Thank you for the thought-provoking question. Based on re-examined calculations, the 1% increase in R is identified as the dominant factor driving the 31%

enhancement in EMI SE for lattice-structured MXene. Although 1% may seem small, in the context of high shielding effectiveness, its absolute value contribution is significant. The lattice architecture enhances EMI shielding through dual mechanisms: (i) Amplified wave absorption due to Rayleigh scattering of GHz electromagnetic waves at micron-scale surface structures; (ii) Enhanced wave reflection originating from additional conductive pathways and multi-reflection events at the patterned interfaces.

The core advantages of the lattice structure: It is not merely a simple "increase in area", but through the carefully designed micro-nano structures, it simultaneously introduces enhanced conductive networks and efficient sub-wavelength scattering mechanisms (Rayleigh scattering).

In response to this comment, the revised version includes: (i) the reasons for the enhancements in SE_A and SE_R, (ii) how the 1% increase in reflection coefficient resulted in a 31% improvement in the EMI shielding effectiveness of the MXene lattice, and (iii) the impacts of increased conductive pathways and enlarged reflection surfaces on EMI shielding performance.

Page 6, Paragraph 1, Line 7-10, in the revised manuscript:

According to Figure S17, the 1% increase in the reflection coefficient (R) indicates that the additional conductive paths introduced by the lattice structure enhance electrical conductivity. This constitutes the primary contributor to the 31% improvement in EMI SE.

Q7: The authors should provide experimental electrical conductivity data for latticed, vacuum-filtered, and flat MXene films. In addition, conductivity and EMI SE values calculated using equation 4 and 5 should be included for better comparison and understanding.

Reply: Thanks you for the insightful suggestion. The experimental electrical conductivity data of the lattice, vacuum filtration and flat MXene films are presented in Table R2(Table S6 in supporting information).

The electrical conductivity of MXene-VAF was measured at 2900 S/cm using a four-probe conductivity meter, according to Equation EMI SE=50+10lg($\frac{\sigma}{f}$)+1.7$t\sqrt{\sigma f}$(5)

$$\text{EMI SE}=50+10\lg\left(\frac{2900}{f}\right)+1.7\times0.0013\times\sqrt{2900\times f}$$

The EMI SE of MXene-VAF averages 56.6 dB in the X-band, calculated from 201 equally spaced frequency points across the 8.2-12.4 GHz range.

The electrical conductivity of flat MXene was measured at 3500 S/cm using a four-probe conductivity meter, according to Equation EMI SE=50+10lg($\frac{\sigma}{f}$)+1.7$t\sqrt{\sigma f}$(5)

$$\text{EMI SE}=50+10\lg\left(\frac{3500}{f}\right)+1.7\times0.0008\times\sqrt{3500\times f}$$

The EMI SE of flat MXene averages 53.5 dB in the X-band, calculated from 201 equally spaced frequency points across the 8.2-12.4 GHz range.

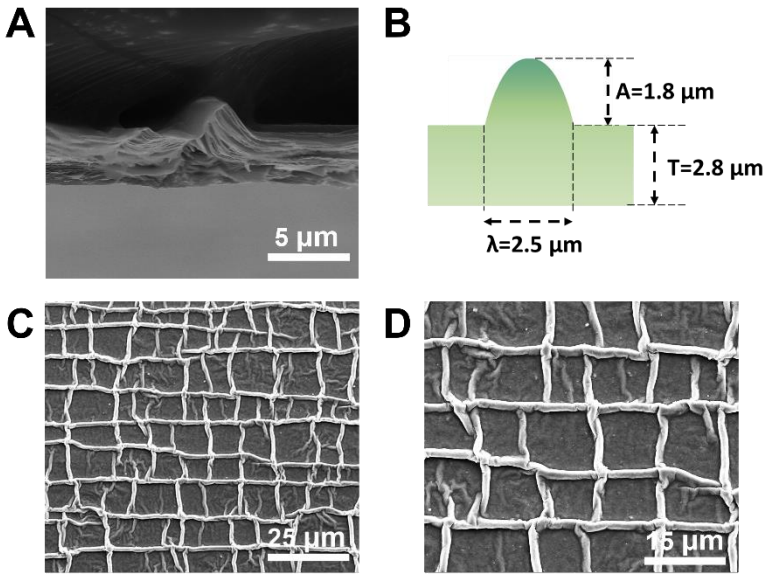

Fig. R9 (Fig. 21 in Supplementary information) (**A**) SEM images of the cross-section for latticed MXene on PI surface. (**B**) The cross-sectional equivalent diagram of the latticed MXene. (**C, D**) SEM image with different magnifications of the latticed MXene.

The electrical conductivity of flat-structured MXene with a thickness of 2.8 μm after

heat treatment was measured as σ_A=3000 S/cm. According to the cross-sectional SEM image of the MXene lattice shown in Figure R9A, the cross-sectional equivalent diagram of the MXene lattice is presented in R9D.

The cross-sectional area S_{A1} of a single fold is:

$$S_{A1}=\int_{1.25}^{1.25}(-1.153x^2+1.8)dx=3.0\ \mu m^2$$

Then the volume V_{A1} of a single fold is:

$$V_{A1}=S_{A1}\times 58\ \mu m=174\ \mu m^3$$

According to Figure R9C, D, five wrinkles along the x-direction and five along the y-direction are observed within a 58×58 μm region. Therefore, within the range of 58×58 μm, the volume φ_A of the lattice is:

$$V_A=174\ \mu m^3\times 10=1740\ \mu m^3$$

$$V_B=(58\times 58\times 2.8)\ \mu m^3=9419\ \mu m^3$$

$$\varphi_A=\frac{1740}{1740+9419}=0.156,\ \varphi_A=\frac{9419}{1740+9419}=0.844$$

$$R=\frac{2.8}{1.8+2.8}=0.6$$

According to Formula $\sigma_{\ latticed\ MXene}=\frac{(\varphi_A+\varphi_B R)}{R[\varphi_A(\varphi_A+\varphi_B R)+\varphi_B]}\sigma_A$ (4)

$$\sigma_{\ latticed\ MXene}=\frac{(0.156+0.844\times 0.6)}{0.6\times[0.156\times(0.156+0.844\times 0.6)+0.844]}\times 3000$$

The calculated σ value of 3498.6 S/cm closely matches the experimentally measured conductivity of 3500 S/cm for latticed MXene, thereby validating the feasibility of Equation (4).

according to Equation EMI SE=$50+10\lg(\frac{\sigma}{f})+1.7t\sqrt{\sigma f}$(5)

The EMI SE of latticed MXene averages 48.2 dB in the X-band, calculated from 201 equally spaced frequency points across the 8.2-12.4 GHz range.

Based on the above calculation results, the theoretical and measured data of MXene-VAF, flat MXene and latticed MXene films are presented in Figure R10.

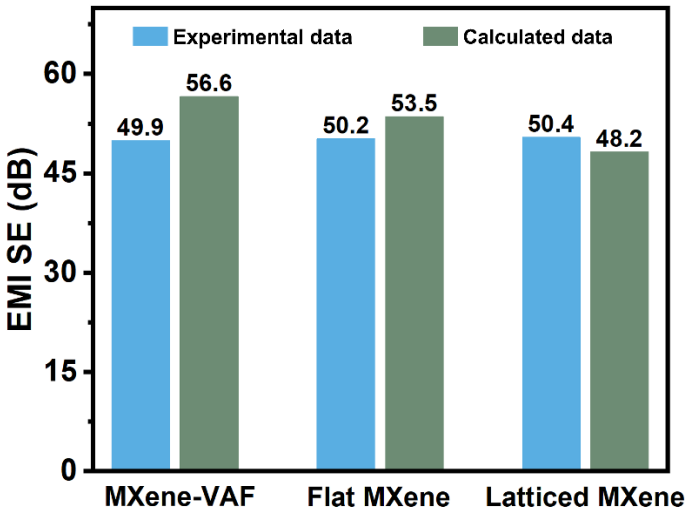

Fig. R10 (Fig. S22 in Supplementary information) Experimental EMI SE and theoretical EMI SE calculated based on Simon formula of MXene-VAF, flat MXene and latticed MXene films.

The calculation results show that the electrical conductivity of the lattice structure has increased from 3000 S/cm to 3498.6 S/cm. The EMI SE calculated by the Simon formula has been improved from 47.3 to 48.2 dB, verifying that the lattice structure can enhance the electromagnetic shielding efficiency of the material. The calculated values of MXene-VAF and Flat MXene are higher than the experimental values, but the calculated value of latticed MXene is lower than the experimental value. The reason is that the Simon formula only considers the relationship between conductivity and shielding efficiency, while surface diffuse reflection caused by the surface structure are not taken into account. In summary, the calculation results are consistent with the test results in Figure 2A and S17: the increase in conductivity and the increase in surface diffuse reflection jointly lead to a higher EMI SE for latticed MXene at the same thickness.

In response to this comment, Figures R9 and R10 have been added to Figure S21 and S22 in the supporting information. The revised version includes the calculated conductivity using Equations 4 and 5, along with the measured conductivity, and the analysis of the results.

Q8: Author should provide the detail discussion on the multiple reflection effect in this study.

Reply: Thank you for the suggestion. In response to this comment, the revised version includes a discussion of multiple reflections.

Page 6, Paragraph 3, Line 22-31 in the revised manuscript:

Additionally, non-uniform electric field distribution is observed in latticed surfaces when subjected to an external electric field, leading to higher power loss density at the lattice (Fig. S23), suggesting that electromagnetic waves are not only subjected to reflection loss but also diffuse reflection on surfaces with structures. Simulations of the EF direction in the y-z plane (Fig. 2G and S24) demonstrates that the direction of the electric field of the lattice structure changes at the raised lattice. This indicates that the formation of the raised structure on the surface facilitates the enhancement of diffuse EM wave scattering, while influencing the electric field distribution at the surface. The potency of the raised lattice structure can be explained by the bandwidth of GHz frequency electromagnetic waves and its interaction with micrometer scale regular structures through Rayleigh scattering[27-30].

Q9: The original and retained values of EMI shielding effectiveness (SE) should be included in the text to demonstrate the long-term stability of the latticed MXene structure for better understanding.

Reply: Thanks you for the excellent advice. In response to this comment, the revised version includes the original and retained values of the EMI shielding effectiveness (SE). Tables R4, R5 and R6 have been added to tables S10, S11 and S12 in the supplementary information.

Table R4 (Supplementary Table 10 in the revised supplementary information) EMI SE of latticed MXene films under different tensile strains.

Tensile strain (%)	Retained EMI SE (dB)
0	81.5

2%	81.5
5%	81.3
8%	81.0
11%	80.3

Table R5 (Supplementary Table 11 in the revised supplementary information) The original and retained values of EMI SE for latticed MXene films under different tensile strains.

Different harsh conditions	Original EMI SE (dB)	Retained EMI SE (dB)
Ultrasound, 2 h	81.5	79.1
Ultrasound, 6 h	81.5	77.7
300 °C, 24 h	81.5	78.5
-196 °C, 24 h	81.5	80.0
pH=1, 24 h	81.5	80.0
Thermal shock, 50 times	81.5	77.8

Table R6 (Supplementary Table 12 in the revised supplementary information) The retained EMI SE of latticed MXene, flat MXene, and MXene-VAF films after exposure to environments at 40°C and 60-80% humidity for different durations.

Sample	Time (months)	Retained EMI SE (dB)
Latticed MXene	0	81.5
	1	80.9
	2	76.5
	3	73.2
	4	70.2
Flat MXene	0	81.5
	1	72.9
	2	60.9

	3	56.9
	4	50.9
MXene-VAF	0	81.7
	1	69.9
	2	58.9
	3	49.9
	4	45.9

In response to this comment, Table R4, R5 and R6 have been added to Table S10, S11 and S22 in the supporting information.

Q10: The term "MXene/PI films" should be clarified: does it refer to latticed MXene or the entire MXene composite? Similarly, the title of Figure 4 should reflect this clarification.

Reply: Thanks you for pointing out the lack of clarity regarding the term “MXene/PI films”. MXene/PI film refers to the entire MXene composite material. In this work, MXene forms a lattice structure on the surface of PI. The testing and characterization conducted in this study were on the MXene/PI composite film. For the EMI shielding performance, the EMI shielding performance is provided by latticed MXene, while PI and PET polymer substrates have insignificant EMI shielding performance (Fig. R1). Therefore, it is named as latticed MXene. The third figure reveals the excellent mechanical properties and the stability under extreme environments, which are attributed to the surface lattice structure and the PI substrate. The fourth figure demonstrates the hydrophobic property and the anti-icing property, which are provided by MXene with a lattice structure. The Joule heating ice removal property is attributed to the surface lattice structure and the PI substrate.

In response to this comment, the section title for Part 3 has been revised to “Joule heating and deicing properties” to maintain consistency with the heading of Part 4.

Q11: In the synthesis section, the authors mention using the HCl/LiF method for

fabricating MXene. However, it is unclear why sonication is necessary, as this process is commonly used for synthesizing single-layer MXene.

Reply: Thanks you for the excellent question. Firstly, we etched the aluminum layer in HCl and LiF to synthesize multilayer MXene. Then, through ultrasonication treatment, MXene was delaminated to obtain single/few-layer MXene nanosheets. Subsequently, the single/few-layer MXene slurry was rapidly concentrated to proceed to the next step of blade coating. Studies have shown that the thickness of a single layer of MXene is only 1.5-2.0 nm. The single layer MXene solution obtained after ultrasonic oscillation is strictly referred to as few-layer MXene, rather than ideal single-layer MXene, which is determined jointly by the inherent properties of the and the material and the preparation process. The surface of the MXene layers contains a large number of unsaturated bonds (such as -O, -OH, -F termination groups), resulting in an extremely high surface energy (>100 mJ/m^2). To reduce energy, the layers will spontaneously stack through van der Waals forces, forming a few-layer structure of 2-5 layers. The -OH terminations on the surface and water molecules or -OH terminations of adjacent layers form hydrogen bond networks (energy≈20 kJ/mol), further promoting interlayer adsorption. In summary, the thermodynamic instability of single-layer MXene leads to the spontaneous stacking of MXene nanosheets.

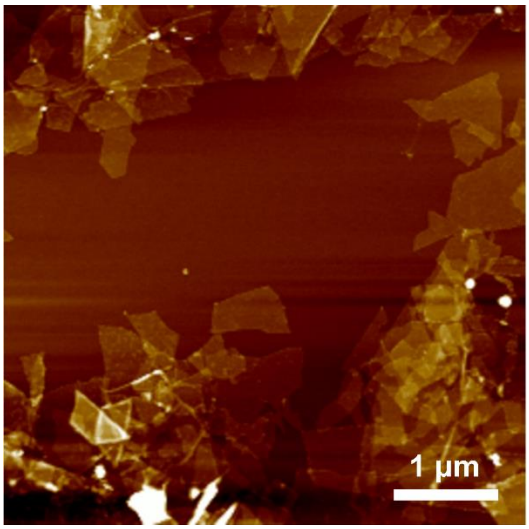

R11. AFM image and of the few-layer $Ti_3C_2T_x$ MXene flakes.

The AFM image of the MXene after ultrasonication is presented in Fig. R11. It was found that the few-layer MXene we prepared was similar to that reported in the literature, as monolayer MXene tended to restack. Therefore, to be rigorous, the MXene prepared after ultrasonication was thus referred to as few-layer MXene.

Q12: References 19 and 33 appear to be identical and should be revised accordingly.

Reply: Thanks you for pointing out this error. We reviewed this error and changed the 33 references in the article to 19. The subsequent reference numbers were then sequentially decreased by 1.

Q13: The authors are encouraged to provide detailed discussions for all figures and subfigures in the supporting information section to enhance the overall clarity and completeness of the manuscript.

Reply: Thanks you for your invaluable input. We have provided detailed discussions for each SI figure in the supporting information section, and the changes made have been highlighted in the supporting information.

Response to Reviewer 2' Comments

Reviewer 2：

Comments: Although the authors have revised the manuscript as suggested, several critical issues remain. There are still unclear points regarding the main advantages of the lattice-structured MXene in terms of properties compared to the reported literature. In addition, the EMI shielding and Joule heating performance comparisons are still very limited.

Reply: We sincerely thank you for your time and for providing these additional constructive comments, which have helped us further improve our manuscript. We have conducted additional analyses and comparisons to better highlight the advantages of our work. Please find our point-by-point responses below.

Q1: The novelty of this work remains unclear. The enhanced EMI shielding performance largely results from the improved electrical conductivity of the lattice-structured MXene. However, achieving high EMI shielding effectiveness (SE) through increased conductivity is already well established in the literature. No fundamentally new mechanism has been introduced. Similar strategies that combine surface patterning with conductivity enhancement have already been reported, e.g., Angew. Chem. Int. Ed. 2022, 61, e202201323. The authors should clarify the novelty of their approach and how it differs from existing methods.

Reply: We sincerely thank the reviewer for this insightful comment. To achieve ultra-thin thickness without compromising shielding performance, it remains a major challenge in this field. To attain high shielding effectiveness with minimal thickness, it is imperative to propose new shielding mechanism. Here, we achieved an ultrathin MXene film (2.8 μm) with a patterned lattice structure, exhibiting the ultrahigh EMI. The unique shielding enhancement mechanism of this structure lies in its dual capability: on one hand, the interlaced lattice provides additional conductive pathways, thereby

enhancing the reflection of electromagnetic waves (EMWs); on the other hand, the uniform micro-nano lattice induces Rayleigh scattering, which further strengthens the absorption of EMWs (Figure R1).

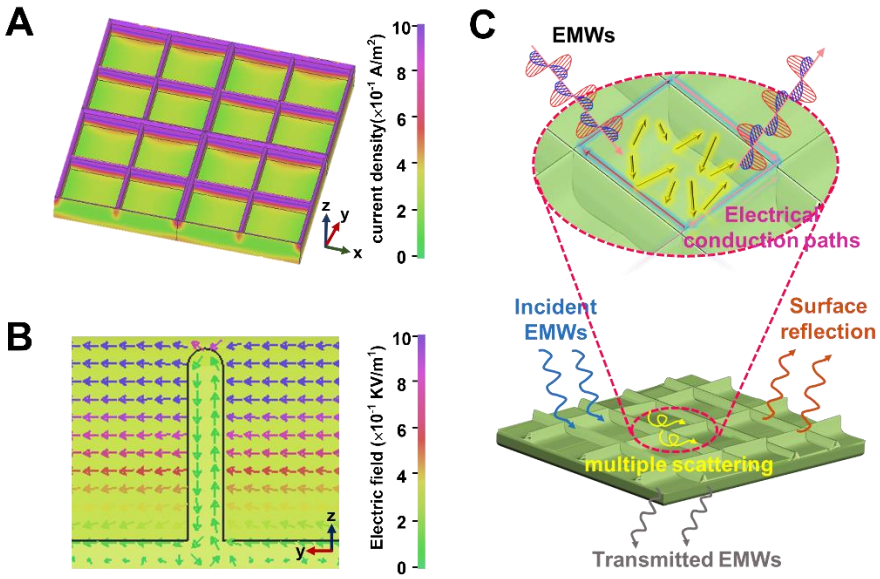

Figure R1. (A) Finite element simulated current density map and (B) electric field direction maps of lattice-structured films at 10 GHz. (C) Schematic of EMI shielding mechanism in the lattice structured MXene film.

There have been some notable studies in this field, such as Angew. Chem. Int. Ed. 2022, 61, e202201323. That work achieved exceptional EMI shielding of 58 dB requiring a thickness of 5 μm, by introducing extensive Ti vacancies via chemical etching, which generated micro-wrinkles and enhanced absorption. Here, we make a great breakthrough to achieve nearly similar EMI SE with only 56% of the thickness. The novelty of our work is summarized as following:

(i) Fabrication approach: Our lattice pattern was achieved through uniform thermal shrinkage of MXene on a polymer surface, whereas Angew. Chem. Int. Ed. 2022, 61, e202201323 utilized chemical etching. Our approach has the great advantage of controlling the wrinkled pattern for the different thickness films.

(ii) Pattern structures: We obtained an interlaced lattice architecture, resembling a crosshatched grid pattern. In contrast, the aforementioned study produced a randomly

wrinkled surface with micro-fold structures. This uniform lattice architecture is vital to achieve the ultrathin yet high-performance EMI.

(iii) Shielding mechanisms: The interconnected ordered lattice in our film provides additional conductive pathways, significantly enhancing the reflection of electromagnetic waves (EMWs) and Rayleigh scattering. The randomly formed micro-wrinkles in Angew. Chem. Int. Ed. 2022, 61, e202201323 makes difficult to form effective conductive networks, thus resulting in limited improvement in electrical conductivity.

Table R1 (Table S1 in Supplementary Information). Thickness and EMI SE values of MXene shielding materials.

Material type	**Thickness (μm)**	**EMI SE (dB)**	**Ref.**
Wrinkled MXene films	5.0	58.0	1
$Mo_2Ti_2C_3T_x$	3.5	23.0	2
$Ti_3C_2T_x$	8.0	26.0	
$Ti_3C_2T_x$	11.0	57.0	
Ti_2CT_x	11.0	50.0	3
V_2CT_x	12.0	46.0	
Nb_2CT_x	10.0	15.0	
$Ti_{1.6}Nb_{0.4}Ct_x$	14.0	50.0	
$Nb_{0.4}V_{1.6}CT_x$	12.0	36.0	
$Ti_3C_2T_x$	14.0	70.0	
Ti_3CNT_x	10.0	55.0	
$Mo_2TiC_2T_x$	9.0	21.0	
$Nb_4C_3T_x$	11.0	26.0	
$Mo_2Ti_2C_3T_x$	13.0	37.0	
MXene/BC	4.0	37.3	4
MXene/PA	20.0	38.9	5
MXene Foam	1.0	29.0	6
	6.0	53.0	
MXene/rGO film	15.0	47.0	7
Ag NWs-MXene-Ag NPs	20.0	71.0	8

MXene/Fe_3O_4@CNTs/TOCNF	18.0	66.0	9
HA/MXene@polypyrrole	14.9	22.6	10
NaOH-treated $Ti_3C_2T_x$ MXene	16.0	49.0	11
Latticed MXene	**0.7**	**38.6**	**This work**
	1.5	**45.7**	
	2.8	**50.4**	
	7.0	**65.7**	
	17.0	**81.5**	

We have included a comparison with relevant literature, including Angew. Chem. Int. Ed. 2022, 61, e202201323, in the manuscript to more clearly demonstrate the novel mechanism of shielding performance enhancement enabled by the lattice-patterned structure.

Page 6, Paragraph 3, Line 32 in the revised manuscript:

Previous works indicated that wrinkled structures can effectively enhance electromagnetic wave absorption, with a 5 μm thick wrinkled MXene film for a shielding effectiveness of 58 dB[31]. Here, we achieved an ultrathin MXene film (2.8 μm) with a patterned lattice structure, exhibiting the nearly similar ultrahigh EMI SE. The unique shielding enhancement mechanism of our lattice architecture lies in its ability to provide additional conductive pathways through the crossed lattices, thereby enhancing the overall electrical conductivity of the film. Simultaneously, the uniform micro/nano lattice configuration induces Rayleigh scattering, which further augments electromagnetic wave absorption. The synergistic enhancement of both reflection and absorption results in a significantly higher total shielding effectiveness in the lattice-patterned MXene compared to other surface-patterned films reported in the field[13, 31, 32].

Q2: The authors compare the EMI performance with limited literature. However, a more comprehensive benchmarking against state-of-the-art MXene shielding materials, particularly those with thicknesses below 20 μm, is missing. The authors should include a plot of EMI SE versus thickness for pristine MXene reported in

the literature in Figure 1f, along with the corresponding numerical data in a supplementary table. This will enable readers to better understand how the lattice-structured MXenes (MXene/PI) in this study compare to previously reported pristine MXene films and allow for a more robust evaluation of their EMI performance.

Reply: We sincerely thank the reviewer for this insightful and constructive comment. We completely agree that a more comprehensive benchmarking against state-of-the-art, ultra-thin pristine MXene films is crucial to better highlight the advantages of our designed MXene/PI lattice structure.

Based on the valuable suggestions from the reviewers, we have added comparisons with state-of-the-art MXene shielding materials in this study. The related references are presented in Table R1 and have been incorporated into Figure 1F (Figure R2) and the Table S1. As clearly demonstrated in the revised Figure 1F, our lattice-structured MXene exhibits electromagnetic interference shielding effectiveness superior to nearly all previously reported EMI shielding films of the same type at comparable thicknesses. This comparison underscores the advancement of our fabrication strategy, which utilizes uniform polymer shrinkage to induce wrinkling and form regularly structured MXene lattices, in achieving exceptional performance in the field of ultra-thin and highly efficient electromagnetic shielding.

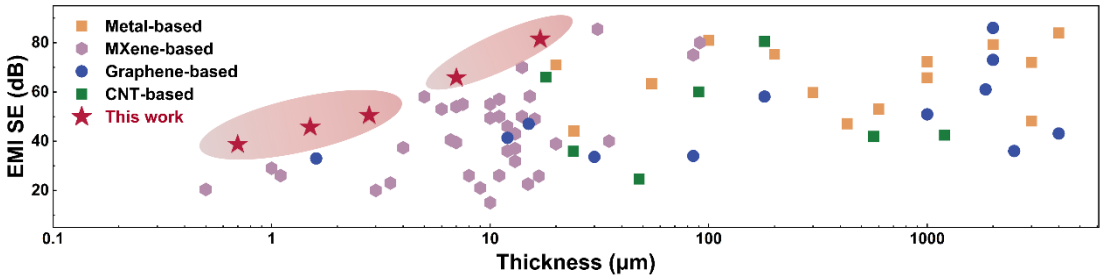

Figure R2 (Figure 1F in manuscript). Comparison of the EMI shielding performance of the lattice-structured MXene with other recently reported EMI shielding materials.

Page 5, Paragraph 2, Line 18 in the revised manuscript:

The lattice-structured MXene exhibits a superior EMI shielding performance,

surpassing most previously reported works, particularly in the field of ultra-thin EMI shielding films, as shown in Fig. 1F and Table S1.

Q3: This is necessary to assess whether any wrinkles form on the PI film after drying. If the pristine PI film does not exhibit wrinkles, it raises concerns about the interfacial interactions between MXene and PI. In such a scenario, the adhesion at the MXene/PI interface may be significantly weakened upon drying, potentially leading to delamination or peeling.

Reply: We thank the reviewer for this excellent suggestion. We agree entirely that providing AFM data for the pristine films is necessary to rule out any ambiguity regarding the origin of the wrinkling and to properly assess the interfacial adhesion.

In response to this comment, we have now provided the AFM height images and corresponding thickness profiles of the pristine PAA film and the pristine PI film (Figure R3).

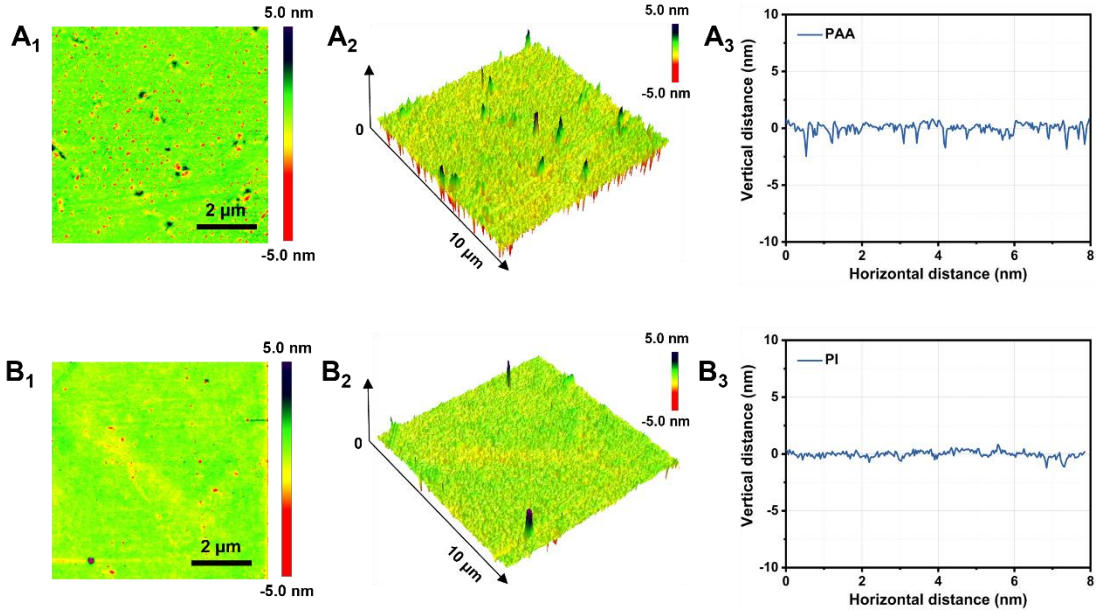

Figure R3 (Figure S7 in Supplementary Information). (A_1) 2D AFM (A_2) 3D AFM images and (A_3) height profiles of the PAA. (B_1) 2D AFM (B_2) 3D AFM images and (B_3) height profiles of the PI.

The new data clearly shows that both the pristine PAA and the fully cured PI films

are smooth and completely free of wrinkles. This observation leads to a key conclusion that the wrinkles observed on the MXene/PI film are not inherent to the PI substrate, but are exclusively formed due to compressive stresses introduced by the MXene layer during the drying process. The fact that the pristine PI film itself is smooth demonstrates that the wrinkling is a direct result of strong interfacial interactions between MXene and PI.

Hydrogen bonding interactions between the polymer and MXene were established even before thermal treatment. During the heating process, partial dissociation of the original hydrogen bonds connecting PAA and MXene occurred. Following the conversion of PAA to PI via dehydration-induced cyclization, new van der Waals interactions and hydrogen bonds were formed between the -OH groups on the MXene nanosheets and the C=O groups in the PI molecular chains[15]. The strong resistance of MXene to delamination from the polyimide (PI) surface was confirmed by the peel stability and ultrasonication test results presented in Section 3 (Figures S30 and S31 in Supplementary Information) of this paper. Furthermore, we have provided a supplementary video (Video S1 in the Supplementary Information) demonstrating the sonication process of MXene/PI, MXene/PET, and MXene-VAF films. The video clearly shows that for the MXene/PET film, the solution begins to turn cloudy after 1 s of sonication, accompanied by the diffusion of MXene into the aqueous solution. For the MXene-VAF material, cracking is observed after approximately 35 s of sonication, followed by gradual clouding of the solution. In contrast, no detachment of MXene is observed for the MXene/PI film even after 6 hours of sonication, and the aqueous solution remains clear (Fig. S32 in the Supplementary Information).

Page 9, Paragraph 2, Line 16 in the revised manuscript:

Video S1 clearly shows that for the MXene/PET film, the solution begins to turn cloudy after 1 s of sonication, accompanied by the diffusion of MXene into the aqueous solution. For the MXene-VAF film, cracking is observed after approximately 35 s of sonication, followed by gradual clouding of the solution. In contrast, no detachment of MXene is observed for the MXene/PI film even after 6 hours of sonication, and the

aqueous solution remains clear (Fig. S32).

Q4: For Figure S34, the authors should provide a video showing the immersion of the lattice MXene in liquid nitrogen, followed by its bendability after removal. MXene films typically become brittle under such conditions and are prone to breaking upon bending. Including this video would help validate the mechanical flexibility and structural integrity of the lattice MXene under extreme conditions.

Reply: We sincerely thank the reviewer for this valuable suggestion. We agree that a direct visual demonstration is the most compelling way to showcase the exceptional mechanical flexibility and structural integrity of our lattice MXene architecture under extreme cryogenic conditions.

As requested we have now provided a video (Video S2 in Supplementary Information) demonstrating the entire process. The free-standing lattice MXene film was immersed in liquid nitrogen and repeatedly folded for over one minute to ensure complete thermal equilibrium. It was then removed and immediately subjected to repeated bending and folding. All procedures were performed without any observable peeling or fracture of the MXene layer.

This video unequivocally demonstrates that our lattice MXene structure retains its outstanding flexibility even at -196 °C, which is a stark contrast to the typical brittleness observed in conventional, dense MXene films under such conditions.

Page 9, Paragraph 3, Line 28 in the revised manuscript:

Video S2 demonstrates that MXene/PI films remain capable of withstanding repeated bending and folding without fracture even after removal from liquid nitrogen immersion, highlighting the application potential of latticed MXene in cryogenic environments.

Q5: In Figure 4a, the temperature was measured using an IR camera. However, due to the low IR emissivity of MXene, this method may not provide accurate surface temperature values. The authors should determine the actual IR

emissivity of their samples and/or use a contact-mode thermocouple for verification. Additionally, images of the samples after Joule heating at 4 V, 5 V, 6 V, and 7 V should be included to evaluate any morphological or structural changes induced by heating.

Reply: We thank the reviewer for raising these critical points regarding temperature measurement accuracy and post-heating morphology. We agree that the low IR emissivity of MXene can pose a challenge for non-contact thermography. We have now performed additional experiments to address both concerns thoroughly.

In direct response to the reviewer's suggestion, we performed a simultaneous calibration of the IR camera reading using a fine-wire K-type thermocouple placed in direct contact with the surface of the MXene film during Joule heating (Figure R4).

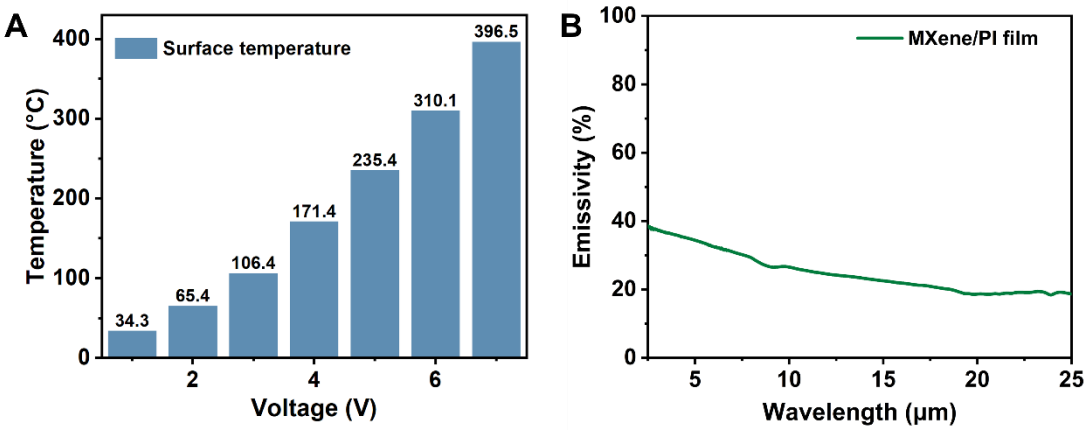

Figure R4 (Figure S38 in Supplementary Information). (A) Surface temperature of the lattice MXene film measured by a thermocouple during Joule heating. (B) The infrared emissivity of MXene/PI films.

In direct response to the reviewer's suggestion, we have provided the infrared emissivity values for both latticed MXene/PI film, with the results presented in Figure R4B. Additionally, we further measured the surface temperature of the lattice MXene film during Joule heating under various voltages. Figure R4A shows the surface temperature of the lattice MXene under different voltages, as measured by a thermocouple thermometer. Compared with Figure 4A in the manuscript, the actual

temperature measured by the thermocouple and the data obtained from the infrared camera are nearly identical. The reason for this agreement is that the emissivity setting in the infrared camera was adjusted to match that of MXene before temperature measurement, meaning the infrared camera was specifically calibrated for our material. This calibrated emissivity value effectively compensates for the intrinsically low emissivity of MXene, enabling the infrared camera to accurately capture the surface temperature.

Page 10, Paragraph 2, Line 10 in the revised manuscript:

The temperature measured by infrared imaging varies from 34.7 to 397.0 °C, showing strong agreement with thermocouple readings (Fig. 4A and S38).

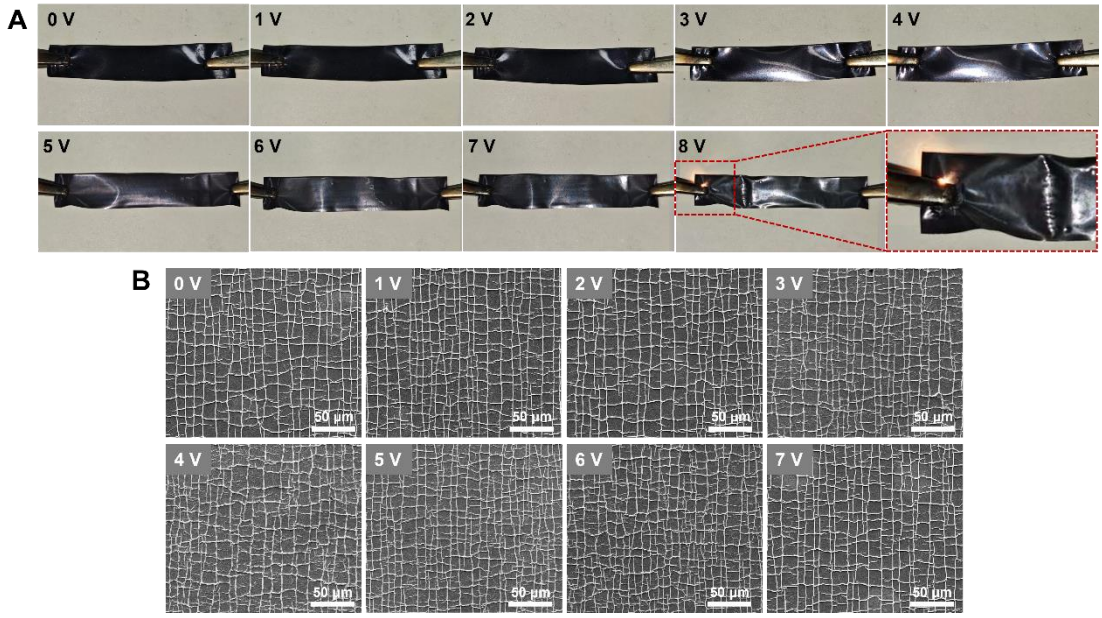

Figure R5 (Figure S41 in Supplementary Information). (A) Optical photos of MXene/PI films under heating at different voltages. (B) SEM images of MXene/PI films under heating at different voltages.

As requested we have supplemented the optical photographs of the MXene/PI film under voltages ranging from 1 to 8 V (Figure R5A). No significant morphological degradation such as cracking delamination or burning was observed at voltages from 1 to 7 V while combustion occurred at the connection between the film and the metal clip at 8 V due to excessive heat. SEM images of the lattice MXene after Joule heating at 1

V to 7 V are presented in Figure R5B. These images reveal negligible changes in the surface morphology of the lattice MXene after being subjected to voltages of 1-7 V compared to its original state. This result demonstrates the exceptional electro-thermal stability and structural integrity of our lattice MXene film under high electrical load.

Page 12, Paragraph 1, Line 8 in the revised manuscript:

The EMI SE of the latticed MXene shows no significant change after several Joule heating deicing cycles (Fig. S40), which can be attributed to the excellent electrothermal stability and structural integrity of the lattice-structured MXene film under high electrical load (Fig. S41).

Q6: In Figure 4d, it is unclear why the lattice MXene exhibits higher hydrophobicity and longer icing time. How does the wrinkled structure enhance hydrophobicity? Additionally, what is the significance of the ice sliding off the film at a 20° tilt under 3 V Joule heating? Furthermore, the authors should also compare the Joule heating performance of the vacuum-filtered and flat MXene films at the same voltage. Are the temperature values comparable?

Reply: We thank the reviewer for these insightful questions, which allow us to further clarify the mechanisms behind the superior performance of our lattice MXene film. We have conducted additional experiments and provided deeper explanations as detailed below.

The enhanced hydrophobicity of the wrinkled structure can be explained by the Cassie-Baxter state. The Cassie-Baxter equation is as follows:

$$\cos\theta_c = f_1 \cos\theta_1 + f_2 \cos\theta_2 \quad (1)$$

According to Figure R6, the lattice was modeled as gridlines with a width of 2.5 μm. The area fraction of the droplet in contact with the latticed MXene, f_1, is given by:

$$f_1 = \frac{2.5\times10\times50}{50\times50} = 0.5,\ f_2 = 1 - f_1 = 1 - 0.5 = 0.5$$

$\theta_c$represents the water contact angle of water droplets on the lattice MXene, θ_1

represents the water contact angle of water droplets on the planar MXene, and θ_2 represents the contact angle of air. Among them, θ_1 = 50.6°, θ_2 = 180°.

$$\cos\theta_c=0.5\times\cos50.6°+0.5\times\cos180°=-0.18$$

$$\theta_c=100.4°$$

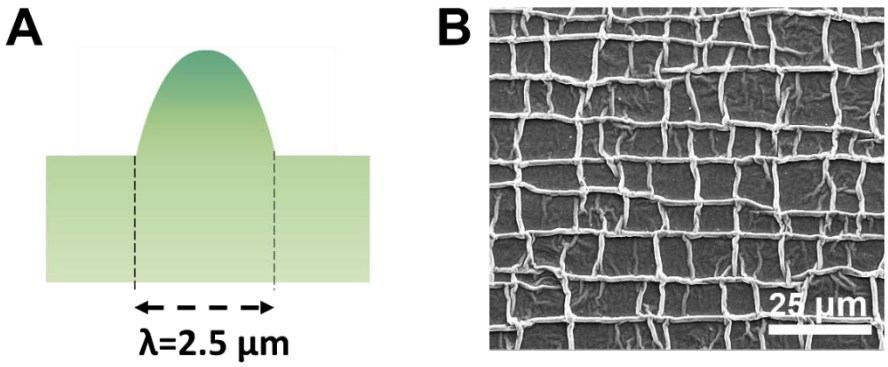

Figure R6. (A) The cross-sectional equivalent diagram of the latticed MXene. (B) SEM image with different magnifications of the latticed MXene.

According to the Cassie-Baxster model, the water contact angle of the lattice-patterned MXene is significantly higher than that of the flat structure (50.6°), demonstrating that the micro-lattice itself is a primary factor enhancing hydrophobicity. Furthermore, heat treatment removed polar groups from the MXene surface, further enhancing its hydrophobicity. In summary, the lattice structure enhances hydrophobicity mainly by trapping air pockets to establish a stable Cassie-Baxter state. The prolonged icing time is a direct consequence of this air layer, which provides thermal insulation. Additionally, our thermal treatment chemically enhanced the intrinsic hydrophobicity of MXene, which works synergistically with the physical structure to ultimately achieve a contact angle of 125° and delayed ice formation.

Page 11, Paragraph 1, Line 10 in the revised manuscript:

The enhancement of hydrophobicity in the latticed MXene is attributed to the combined effect of its unique lattice-patterned structure and the removal of surface polar groups through heat treatment.

Page 11, Paragraph 1, Line 16 in the revised manuscript:

The delayed icing is attributed to the wrinkled morphology of the lattice structure, which facilitates the formation of a stable air cushion beneath the water droplet. This air layer reduces solid-liquid contact and effectively impedes thermal transfer.

The significance of the ice-shedding experiment at a 20° tilt under 3 V Joule heating lies in its demonstration of a synergistic passive-active de-icing strategy, which is highly desirable for practical applications. The combination of low voltage and a minimal tilt angle means that even a slight inclination of 20° is sufficient for gravity to overcome the significantly weakened ice adhesion force, resulting in complete ice removal. This confirms an energy-efficient and effective de-icing capability, as the process requires neither high voltage nor mechanical force. The practical implications of this feature are substantial, particularly in applications where energy efficiency, lightweight design, and autonomous operation are critical. For example, this technology could be applied to aircraft wings and wind turbine blades to prevent ice accumulation without demanding high energy consumption or mechanical intervention. Similarly, it could be integrated into solar panels, power transmission equipment, and outdoor surveillance systems to ensure reliable performance in cold and icy environments. The ability to achieve rapid de-icing at low tilt angles and low voltages also makes it suitable for applications with spatial or structural constraints, such as drones and automotive sensors. By enabling efficient ice removal without complex hardware or significant energy input, this passive-active de-icing strategy offers a practical solution for maintaining operational safety and functionality across a wide range of industrial and environmental conditions.

Page 12, Paragraph 1, Line 4 in the revised manuscript:

This demonstrates that latticed MXene exhibit low ice adhesion and efficient de-icing capabilities under low voltage and slight inclination, indicating their energy-saving potential and practical applicability in anti-icing and de-icing systems.

As requested, we have now compared the Joule heating performance of latticed

MXene film, the vacuum-filtered MXene film and flat MXene film under the same applied voltages. The resulting temperature data is presented in Figure R7A.

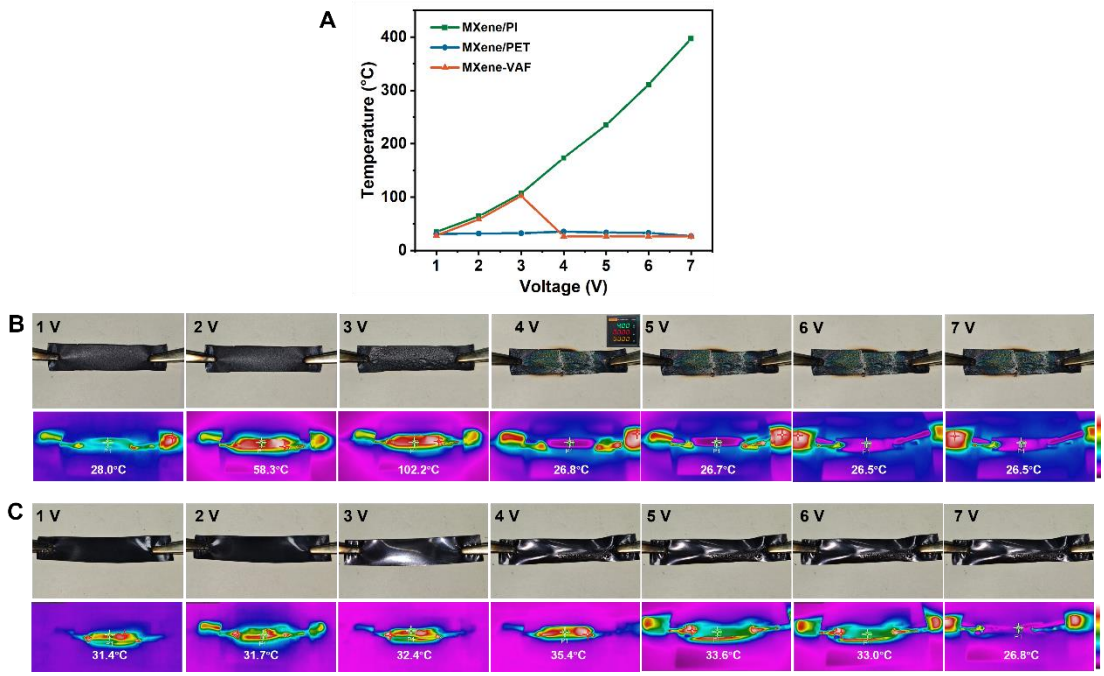

Figure R7 (Figure S37 in Supplementary Information). (A) The temperatures of MXene/PI, MXene/PET and MXene-VAF films at different voltages. The IR thermal images of the (B) MXene-VAF and (C) MXene/PET films at different driving voltages.

The temperature of the MXene-VAF film increases with applied voltage in the range of 1-3 V. However, when the voltage further increases, the MXene-VAF fractures due to excessive heating (Figure R7B). In contrast, the temperature of the MXene/PET film shows no significant change with increasing voltage. This is because the flat MXene layer delaminates from the PET substrate upon mild Joule heating, preventing the formation of a continuous conductive pathway (Figure R7C). In contrast, the lattice-structured MXene/PI film exhibits stable and controllable Joule heating performance even at higher voltages. This can be attributed to the strong interfacial bonding between the MXene and the PI substrate, which prevents delamination and maintains electrical continuity under thermal stress. Furthermore, the outstanding thermal stability of the PI substrate (as demonstrated in Figure 33 in supporting information) enables the hybrid film to withstand elevated temperatures without structural degradation. As a result, the

temperature of the MXene/PI film increases steadily and reversibly with applied voltage, highlighting its potential for reliable operation in electrothermal applications. The combination of robust interfacial adhesion, high thermal tolerance, and consistent electrical performance underscores the advantage of the MXene/PI design over MXene-VAF and MXene/PET film.

Page 10, Paragraph 2, Line 5 in the revised manuscript:

In contrast, the MXene-VAF fractures at 4 V owing to overheating, while the temperature of the MXene/PET film shows no significant change with increasing voltage, owing to the delamination between MXene and PET during heating (Fig. S37).

In response to the reviewer's comment, we have supplemented the comparison with state-of-the-art materials possessing Joule heating performance, as newly provided in Table R2. Additional supporting references are included in Table S13 of the Supplementary Information and Figure 4C of the manuscript.

Table R2 (Table S13 in Supplementary Information). Joule thermal properties comparison of MXene/PI films and other materials reported in literature.

Material type	Voltage (V)	Temperature (°C)	Ref.
MXene-GNs/ANF	4	160.0	13
MXene@CGA/Ag NPs	4	114.1	14
AMLM-PM foam	5	42.5	15
PPF/TCT composite	5	104.8	16
Liquid metal/poly(urethane-urea) composite	2	61.3	17
MXene/PANI/PDA	5	94.0	18
CMOF/SBR/CNT/SBR	10	152.0	19
Carbon fabrics of Kevlar fibres	5	180.0	20
Carbon black/graphene/nickel polyimide foam	3	30.4	21
	5	43.2	
	7	64.8	
	9	89.2	

ES-welded AgNW network	4	80.0	22
Latticed MXene	**1**	**34.7**	**This work**
	2	**64.1**	
	3	**107**	
	4	**173.6**	
	5	**235.2**	
	6	**311**	
	7	**397**	

References

1. Ying, M. F. et al. Wrinkled Titanium Carbide (MXene) with Surface Charge Polarizations through Chemical Etching for Superior Electromagnetic Interference Shielding. *Angew. Chem. Int. Ed*. **61**, e202201323 (2022).
2. Shahzad, F. et al. Electromagnetic interference shielding with 2D transition metal carbides (MXenes). *Science* **353**, 1137-1140 (2016).
3. Han, M. K. et al. Beyond $Ti_3C_2T_x$: MXenes for electromagnetic interference shielding. *ACS nano*, **14**, 5008-5016 (2020).
4. Wan, Y. Z. et al. Ultrathin, strong, and highly flexible $Ti_3C_2T_x$ MXene/bacterial cellulose composite films for high-performance electromagnetic interference shielding. *ACS nano* **15**, 8439-8449 (2021).
5. Cheng, Z. et al. Multifunctional MXene-based composite films with simultaneous terahertz/gigahertz wave shielding performance for future 6G communication. *J. Mater. Chem. A*. **11**, 5593-5605.
6. Liu, J. et al. Hydrophobic, Flexible, and Lightweight MXene Foams for High-Performance Electromagnetic-Interference Shielding. *Adv Mater.* **29**, 1702367 (2017).
7. Tang, X. W. et al Ultrathin, flexible, and oxidation-resistant MXene/graphene porous films for efficient electromagnetic interference shielding. *Nano Res.* **16**, 1755-1763 (2023).
8. Qu, Y. F. et al. Multifunctional AgNWs@MXene/AgNFs electromagnetic shielding

composites for flexible and highly integrated advanced electronics. *Compos. Sci. Technol.* **230**, 109753 (2022).

9. Ma, Z. K. Gradient Layered MXene/Fe_3O_4@CNTs/TOCNF Ultrathin Nanocomposite Paper Exhibiting Effective Electromagnetic Shielding and Multifunctionality. *Nano Res.* **17**, 8233-8242 (2024).
10. Xiong, J. H. et al. Multifunctional Nacre-Like Nanocomposite Papers for Electromagnetic Interference Shielding via Heterocyclic Aramid/MXene Template-Assisted In-Situ Polypyrrole Assembly. *Nano-Micro Lett.* **17**, 53 (2024).
11. Duan, J., Liu, Z., Wang, X. C., Enhanced electromagnetic shielding and absorption in $Ti_3C_2T_x$ MXene films via hydroxyl functionalization and interlayer spacing control. *Surf Coat Tech.* **513**, 132503 (2025).
12. Cheng, Y. et al. Hierarchically porous polyimide/$Ti_3C_2T_x$ film with stable electromagnetic interference shielding after resisting harsh conditions. *Sci. Adv*. **7**, eabj1663 (2021).
13. Yele, M. et al. Integrated structural-functional MXene-GNs/ANF flexible composite film with enhanced thermal conductivity and electromagnetic interference shielding performance. *J. Mater. Sci. Technol*. **241**, 200-210 (2025).
14. Tan, T. et al. Long-term antioxidant MXene@CGA/Ag NPs self-assembled fabric for low infrared emissivity, electromagnetic interference shielding, and dual-mode heating. *Appl. Surf. Sci*. **712**, 164201 (2025).
15. Li, X. F. et al. Inter-Skeleton Conductive Routes Tuning Multifunctional Conductive Foam for Electromagnetic Interference Shielding, Sensing and Thermal Management. *Nano-Micro Lett.* **17**, 52 (2025).
16. Wei, J. S. et al. Sandwich structured cellulose-based composite for electromagnetic interference shielding, infrared stealth and Joule heating. *Carbohydr. Polym*. **367**, 123979 (2025).
17. Ma, R.-Y. et al. Highly stretchable liquid metal/poly(urethane-urea) composite with self-healing ability for electromagnetic interference shielding. *Compos Part B-Eng*. **306**, 112808 (2025).
18. Chen, H. L. et al. Advanced Textiles Inspired by Leaf Structure for Enhanced

Personal Electromagnetic Protection and Thermal Management. *ACS Appl. Nano Mater*. **8**, 7140-7153 (2025).

19. Dehghani, A., Sambyal, P., Arjmand, M. et al. Flexible rubber-based nanocomposite with superior electromagnetic interference shielding and joule heating. *Carbon*, **238**, 120180 (2025).
20. Singh, K., Baheti, V. et al. EMI shielding and joule heating applications of woven and nonwoven activated carbon fabrics of Kevlar fibres. *Anal. Appl. Pyrolysis.* **188**, 107041 (2025).
21. Wang, Y. G. et al. Multifunctional rigid polyimide foams with outstanding EMI shielding and wave absorption via densification strategy. *J. Mater. Sci. Technol*. **227**, 155-163 (2025).
22. Zhu, C. C. et al. Facile electrospray nanowelding process for high-performance and tailored silver nanowire networks. *Appl. Surf. Sci.* **689**, 162465 (2025).